Journal of Applied Physics

RESEARCH ARTICLE | MARCH 25 2024

Performance of normally off hydrogen-terminated diamond field-effect transistor with Al_2O_3/CeB_6 gate materials

Zhang Minghui ; Wang Wei ; Chen Genqiang; Xie Rui; Wen Feng ; Lin Fang; Wang Yanfeng; Zhang Pengfei; Wang Fei ; He Shi; Liang Yuesong; Fan Shuwei ; Wang Kaiyue; Yu Cui; Min Tai ; Wang Hongxing

J. Appl. Phys. 135, 125702 (2024)
https://doi.org/10.1063/5.0185805

AIP Publishing

Journal of Applied Physics | ARTICLE | pubs.aip.org/aip/jap

Performance of normally off hydrogen-terminated diamond field-effect transistor with Al_2O_3/CeB_6 gate materials

Cite as: J. Appl. Phys. **135**, 125702 (2024); doi: 10.1063/5.0185805
Submitted: 2 November 2023 · Accepted: 23 February 2024 ·
Published Online: 25 March 2024

Zhang Minghui,[1] Wang Wei,[1,a)] Chen Genqiang,[1] Xie Rui,[1] Wen Feng,[1] Lin Fang,[1] Wang Yanfeng,[1] Zhang Pengfei,[1] Wang Fei,[1] He Shi,[1] Liang Yuesong,[1] Fan Shuwei,[1] Wang Kaiyue,[2] Yu Cui,[3] Min Tai,[4] and Wang Hongxing[1]

AFFILIATIONS

[1]Key Laboratory of Physical Electronics and Devices, Ministry of Education, School of Electronic Science and Engineering, Xi'an Jiaotong University, Xi'an, Shaanxi 710049, China
[2]School of Materials Science and Engineering, Taiyuan University of Science and Technology, Taiyuan, Shanxi 030024, China
[3]National Key Laboratory of Application Specific Integrated Circuit, Hebei Semiconductor Research Institute, Shijiazhuang, Hebei 050051, China
[4]State Key Laboratory for Mechanical Behavior of Materials, Center for Spintronics and Quantum System, School of Materials Science and Engineering, Xi'an Jiaotong University, Xi'an, Shaanxi 710049, China

[a)]**Author to whom correspondence should be addressed:** wei_wang2014@mail.xjtu.edu.cn

ABSTRACT

In this work, we demonstrate a hydrogen-terminated diamond (H-diamond) field-effect transistor (FET) with Al_2O_3/CeB_6 gate materials. The CeB_6 and Al_2O_3 films have been deposited by electron beam evaporation technique, sequentially. For the 4/8/12/15 μm gate length (L_G) devices, the whole devices demonstrate distinct p-type normally off characteristics, and all the threshold voltage are negative; all the absolute values of leakage current density are 10^{-4} A/cm^2 at a V_{GS} of −11 V, exhibiting a relatively low leakage current density compared with CeB_6 FETs, and this further demonstrates the feasibility of the introduction of Al_2O_3 to reduce the leakage current density; the maximum drain–source current density is −114.6, −96.0, −80.9, and −73.7 mA/mm, which may be benefited from the well-protected channel. For the 12 μm L_G devices, the saturation carrier mobility is 593.6 cm^2/V s, demonstrating a good channel transport characteristic. This work may provide a promising strategy for the application of normally off H-diamond FETs significantly.

I. INTRODUCTION

As an ultra-wide bandgap semiconductor, diamond exhibits the advantages of ultrahigh breakdown field strength, high carrier mobility, exceptionally high thermal conductivity, good corrosion and radiation resistance, etc.[1–3] These excellent characteristics enable diamond-based electronics devices to work safely and stably in the extreme environment, such as high frequency, high pressure, high temperature, and strong radiation. Nevertheless, the development of diamond-based electronic devices has been greatly hampered by the traditional doping technique due to the high activation energies of the dopants (boron of 370 meV and phosphorus of 650 meV).[4] Fortunately, under the condition of C–H bond and negative adsorbates [such as O_2^-, $O_2^-(H_2O)_n$, etc.], hydrogen-terminated diamond (H-diamond) with two-dimensional hole gas (2DHG) accumulation layer comes into view, demonstrating a carrier density of 10^{12}–10^{14} cm^{-2} and a carrier mobility of 10–300 cm^2/V s.[5–8] To date, researchers have made significant progress on H-diamond field-effect transistors (FETs), such as carrier mobility of 680 cm^2/V s,[1] current density of 1.3 A/mm,[9] power density of 4.2 W/mm,[10] maximum oscillation frequency of 120 GHz,[11] cut-off frequency of 70 GHz,[12] and breakdown voltage of V (Ref. 13).

For the application of H-diamond FETs, energy saving and safety protection require the normally off operation. As presented in our previous article, a low work function material is considered to be an effective technique to realize normally off H-diamond FETs.[14] In addition, the preliminary work has fully verified the feasibility of normally off H-diamond FETs with CeB_6 material, which exhibits the advantages of low work function, good chemical stability, high melting point, etc.[15] The device demonstrates good electrical characteristics, yet the absolute value of the leakage current density (J) is large. In order to reduce the J, Al_2O_3 is a good candidate, which demonstrates a large valence band offset with H-diamond.[16–19] Thus, the Al_2O_3/CeB_6 gate material has been utilized in this work. To the best of the author's knowledge, few reports have been made on H-diamond FET with Al_2O_3/CeB_6 gate material.

In this work, the fabrication of the $Al/Al_2O_3/CeB_6$ H-diamond FET has been performed, and its electrical characteristics have been evaluated.

II. EXPERIMENTAL

The fabrication process, cross-sectional schematic, band diagram of gate voltage (V_{GS}) = 0 V, band diagram of $|V_{GS}| > |$threshold voltage (V_{TH})$|$, and device top view of the $Al/Al_2O_3/CeB_6$ H-diamond FET are demonstrated in Fig. 1. In this experiment, a (100) high pressure high temperature (HPHT) single crystal diamond with dimensions of $3 \times 3 \times 0.5\ mm^3$ was utilized as the substrate. First, before the epitaxial layer growth, the substrate was cleaned with mixed acid solutions of H_2SO_4:HNO_3 = 1:1 at 250 °C for 1h to remove the non-diamond contaminates, and then, the substrate was immersed in acetone, alcohol, and de-ionized water sequentially for ultrasonic cleaning, which was dried by nitrogen flow. Second, a 200 nm undoped epitaxial layer was grown on the cleaned substrate by microwave plasma chemical vapor deposition (MPCVD) technique with a gas flow, CH_4/H_2 ratio, temperature, pressure, and power of 500 SCCM, 1%, 900 °C, 100 Torr, and 1 kW, respectively. Furthermore, the CH_4 flow was set to zero, and the substrate was irradiated by hydrogen plasma for the formation of an H-diamond surface with 2DHG conduction channel for at least 20 min.[15] Third, 150 nm Au was adopted as the source/drain ohmic contact electrodes fabricated by photo-lithography, electron beam evaporation (EB), and standard lift-off technique. Fourth, the nonactive region of the substrate was oxidized by 15 min ultraviolet ozone treatment with UV wavelengths of 254 and 185 nm. Finally, 150/30/30 nm $Al/Al_2O_3/CeB_6$ gate electrodes were fabricated by photolithography, EB, and lift-off techniques. The dimensions of the devices are the gate length (L_G) of 4/8/12/15 μm, gate width (W_G) of 100 μm, and source–drain length (L_{SD}) of 20 μm. The characteristics were characterized by a semiconductor analyzer Agilent B1505 A at room temperature.

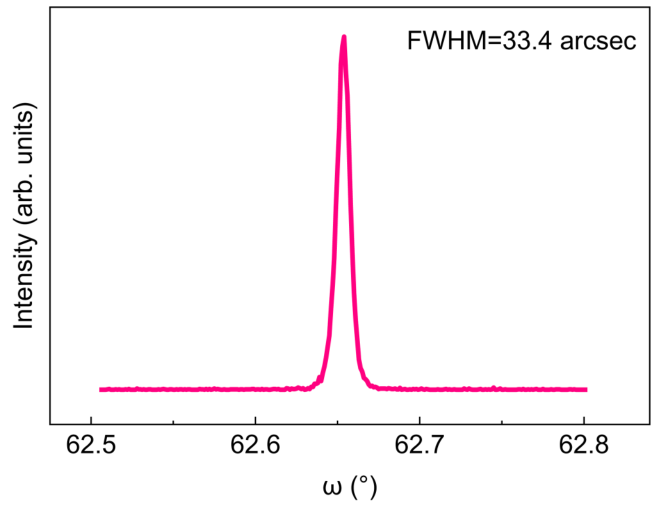

FIG. 2. XRD result of H-diamond.

III. RESULTS AND DISCUSSION

The H-diamond has been characterized by x-ray diffraction (XRD) technique, as demonstrated in Fig. 2. The full width at half

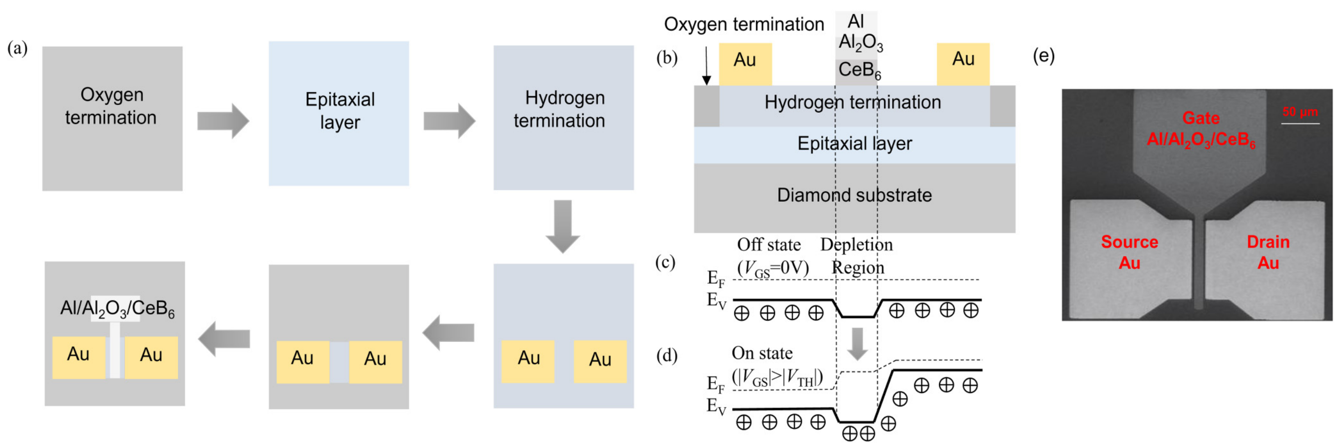

FIG. 1. $Al/Al_2O_3/CeB_6$ H-diamond FET: (a) fabrication process, (b) cross-sectional schematic, (c) band diagram of V_{GS} = 0 V, (d) band diagram of $|V_{GS}| > |V_{TH}|$, (e) device top view.

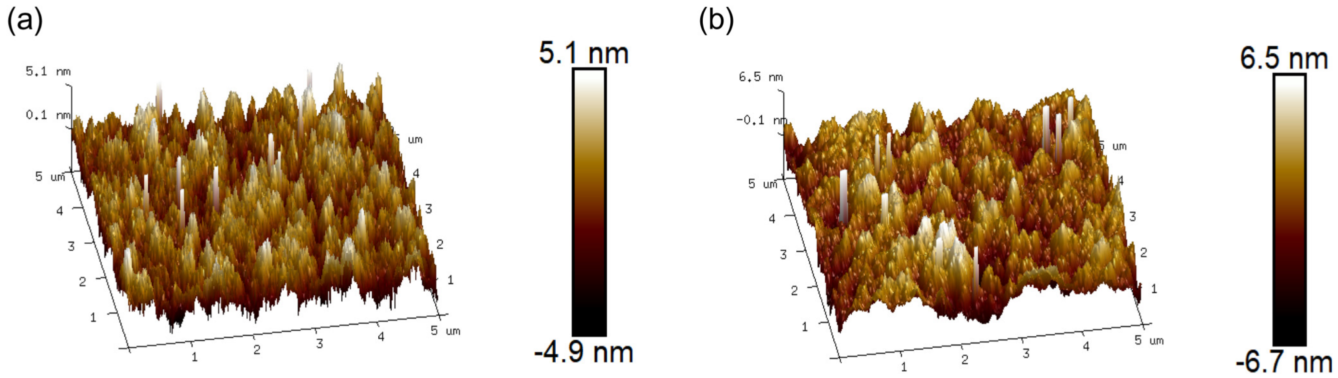

FIG. 3. AFM topography image with a scanning size of 5 × 5 μm^2: (a) Al_2O_3 and (b) CeB_6.

maximum (FWHM) is 33.4 arcsec, indicating a high quality of H-diamond.

In addition, CeB_6 and Al_2O_3 have been characterized by atomic force microscopy (AFM) and x-ray photoelectron spectroscopy (XPS) techniques, respectively. In Fig. 3, the root mean square roughness is 1.10 and 1.36 nm for the Al_2O_3 and CeB_6 materials with a scanning size of $5 \times 5\,\mu m^2$, illustrating an adequate morphology for device fabrication. The XPS spectra of

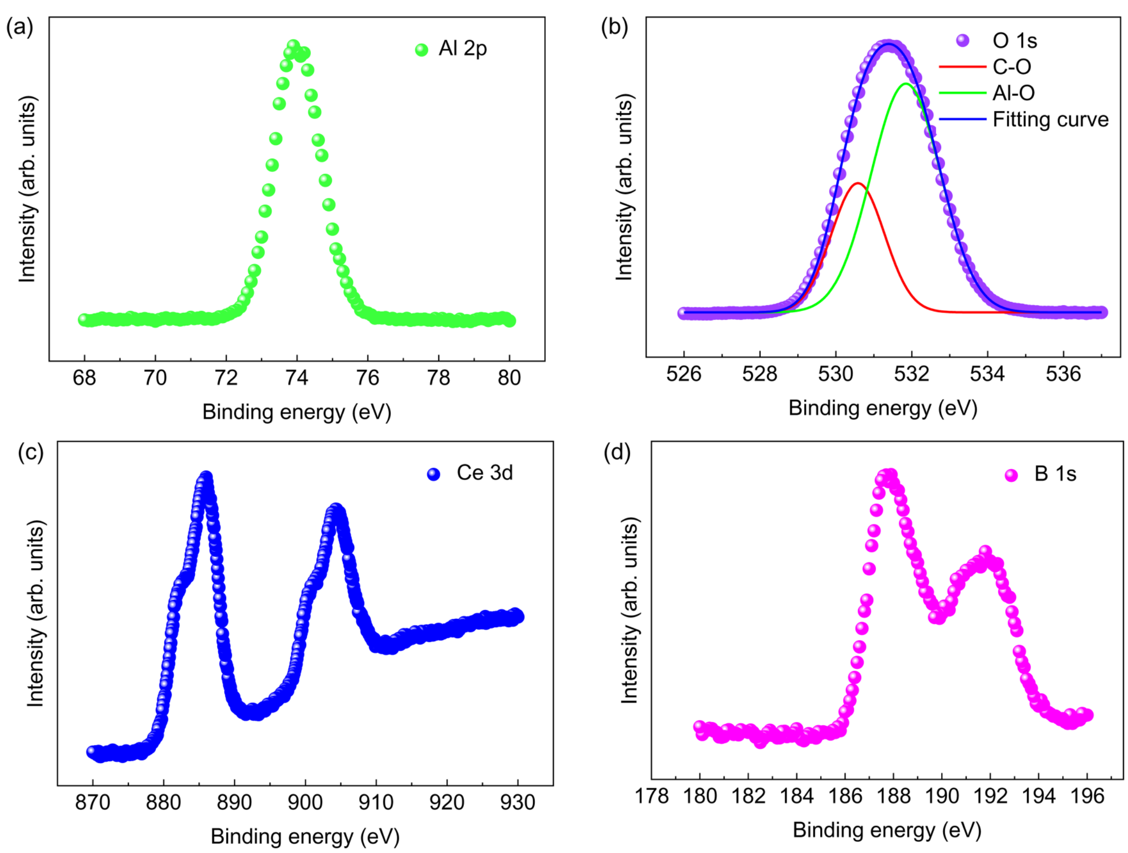

FIG. 4. High resolution XPS spectra of (a) Al 2p and (b) O 1s obtained from the Al_2O_3, (c) Ce 3d, and (d) B 1s obtained from the CeB_6.

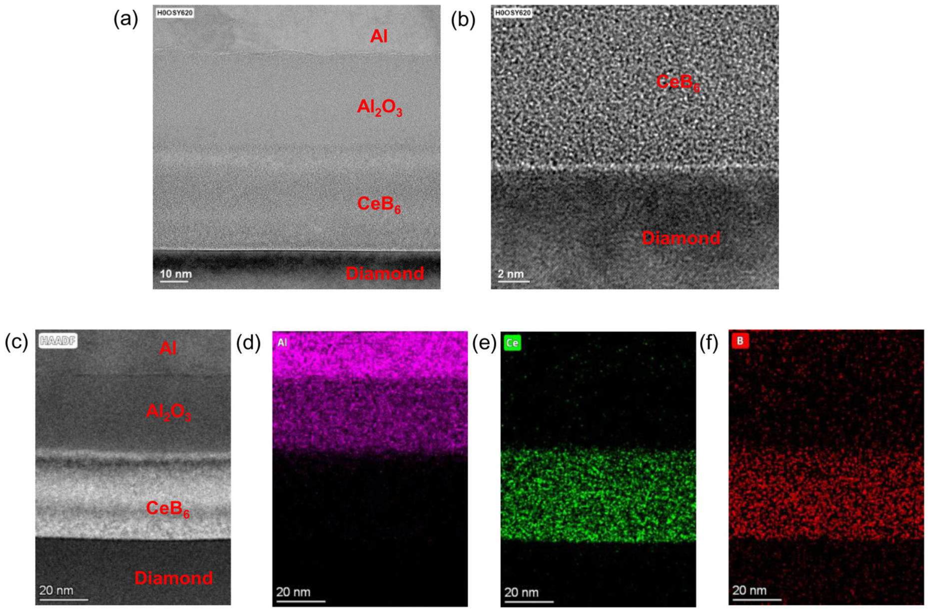

FIG. 5. TEM result of $Al/Al_2O_3/CeB_6$ H-diamond: (a)–(c) cross-sectional image with sizes of 10, 2, and 20 nm, (d)–(f) EDX elemental mapping of Al, Ce, and B, respectively.

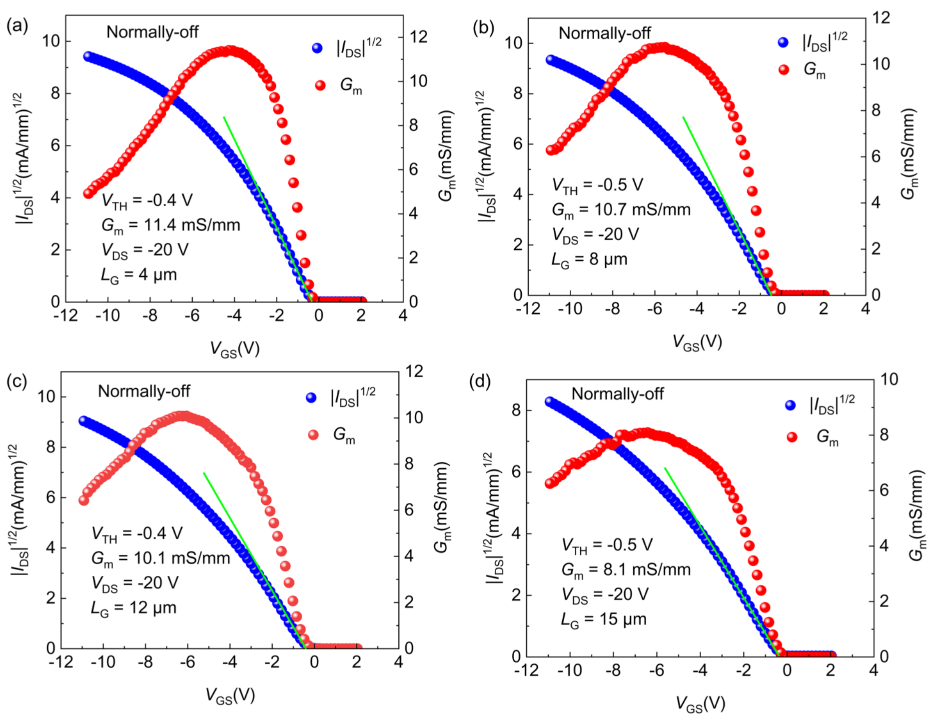

FIG. 6. Transfer characteristics ($|I_{DS}|^{1/2}/G_m$–V_{GS}) of the $Al/Al_2O_3/CeB_6$ H-diamond FET (a)–(d) with L_G of 4, 8, 12, and 15 μm, respectively.

Al_2O_3 are demonstrated in Figs. 4(a) and 4(b). The Al 2p spectrum located at 73.9 eV corresponds to Al–O. And, the O 1s spectrum has been fitted with the Gauss function. The peak located at 530.59 eV belongs to C–O, and the peak located at 531.86 eV corresponds to Al–O. The XPS spectra of CeB_6 are demonstrated in Figs. 4(c) and 4(d). There are two peaks located at 886.0 and 904.3 eV for the Ce 3d spectrum and also two peaks of 187.9 and 191.8 eV for B 1s spectrum.

Furthermore, as shown in Fig. 5, the interface property has been characterized by transmission electron microscopy (TEM) technique, and the composition of the cross section of the Al/Al_2O_3/CeB_6/H-diamond has also been characterized by energy dispersive x-ray analysis (EDX) technique. The TEM result demonstrates a good interface and a uniform distribution of Al, Ce, and B.

The V_{TH} and transconductance (G_m) characteristics of Al/Al_2O_3/CeB_6 H-diamond FET are demonstrated in Fig. 6. For the 4/8/12/15 μm L_G devices, the V_{TH} are −0.4, −0.5, −0.4, and −0.5 V extracted from the curve of drain–source current (I_{DS}) and V_{GS},[18] demonstrating normally off characteristics for the whole devices. The experimental results further verify the effectiveness of the low work function material to realize normally off H-diamond FETs. In addition, G_m are slightly higher than our previous work with values of 11.4, 10.7, 10.1, and 8.1 mS/mm,[4,14] indicating a comparatively good control of V_{GS} on the I_{DS}.

As presented in Fig. 7, distinct saturation and pinch-off characteristics are observed, and $|I_{DS}|$ increases with the increased $|V_{GS}|$, indicating a p-type channel with hole carriers under the Al/Al_2O_3/CeB_6 materials. The maximum I_{DS} (I_{DSmax}) are −114.6, −96.0, −80.9, and −73.7 mA/mm at a drain–source voltage (V_{DS}) of −20 V and V_{GS} of −11 V for the 4/8/12/15 μm L_G devices. Obviously, $|I_{DSmax}|$ decreases with an increase in L_G. In addition, the relatively high I_{DSmax} can be attributed to the well-protected conduction channel, which is not degraded remarkably by EB technique.

Figure 8 presents the J of the Al/Al_2O_3/CeB_6 H-diamond FET with L_G of 4, 8, 12, and 15 μm, respectively. At the V_{GS} of 0 V, all the J values are as low as 10^{-7} A/cm^2. The J demonstrates a relatively low value of 1.2×10^{-4}, 2.0×10^{-4}, 2.2×10^{-4}, and 4.6×10^{-4} A/cm^2 at a V_{GS} of −11 V, and this result shows that the leakage current density increases with the increased gate length, yet all the values are around 10^{-4} A/cm^2. Accordingly, the Al_2O_3/CeB_6 gate dielectric is not excellent, but it seems to be ok. In addition, the reason behind the increased leakage current density may be ascribed to the uneven

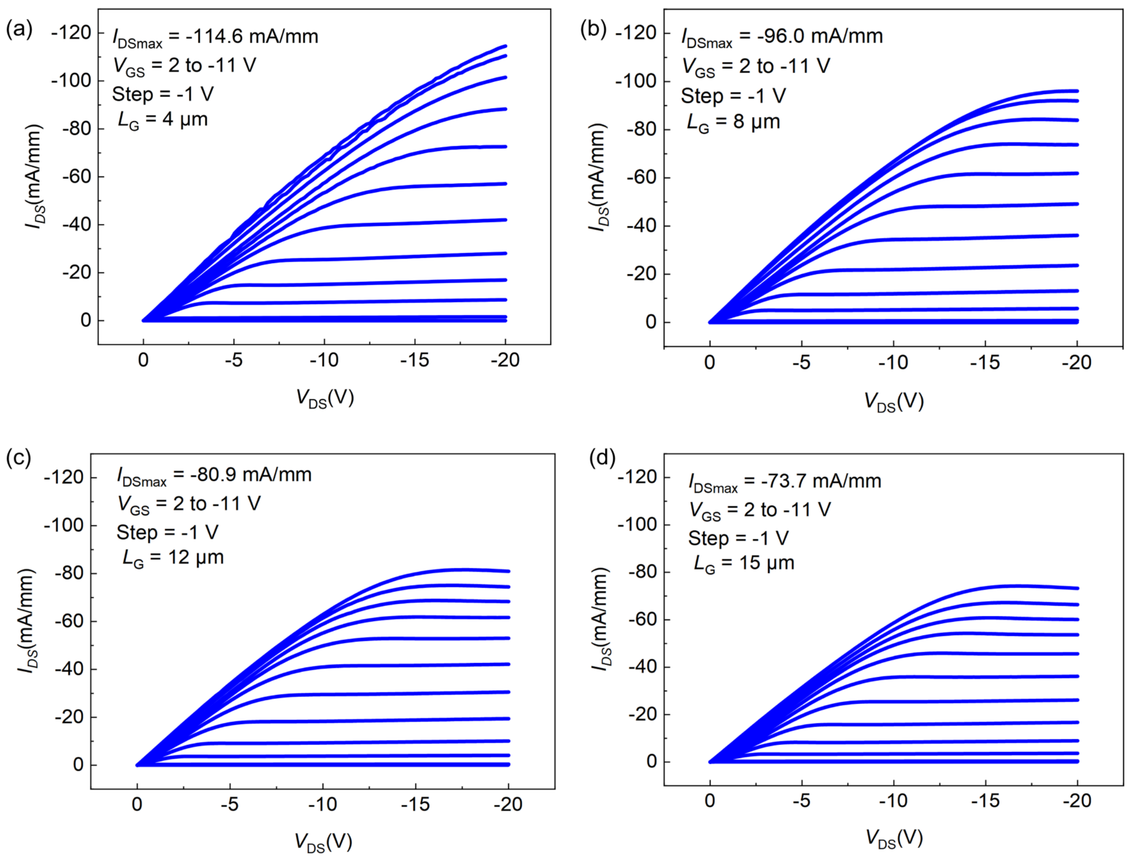

FIG. 7. Output characteristics (I_{DS}–V_{DS}) of the Al/Al_2O_3/CeB_6 H-diamond FET (a)–(d) with L_G of 4, 8, 12, and 15 μm, respectively.

Al_2O_3/CeB_6 gate dielectric. Compared with our previous work, the J of the $8\,\mu m$ L_G CeB_6 FET is 2.4×10^{-3} A/cm^2 @$V_{GS} = -8$ V,[15] and the J of the $8\,\mu m$ L_G Al_2O_3/CeB_6 FET is 3.3×10^{-5} A/cm^2 @$V_{GS} = -8$ V. Even when the V_{GS} increases to -11 V, the J of the $8\,\mu m$ L_G Al_2O_3/CeB_6 FET is 2.0×10^{-4} A/cm^2. All this demonstrates that the introduction of Al_2O_3, indeed, have an effect on reducing the leakage current density.[15]

As shown in Fig. 9, the on/off ratio, subthreshold swing (SS), the capacitance (C_{GS}), the flatband voltage (V_{FB}), the carrier density (ρ) and the saturation carrier mobility (μ_{sat}) characteristics of the $12\,\mu m$ L_G devices are evaluated. The on/off ratio reaches up to around 10^9, which is high enough for practical applications. The SS is extracted to be 120 mV/dec, demonstrating a relatively fast transition rate between on and off states. The C_{GS} is $0.06\,\mu F/cm^2$, indicating that the quality of the CeB_6/Al_2O_3 material is not excellent, which may be improved in our future work. The V_{FB} is calculated to be -1.69 V based on the relationship of $d^2C_{GS}/d^2V_{GS} = 0$.[20] Furthermore, the C_{GS}–V_{GS} curve shifts to the negative direction corresponding to the position of $V_{GS} = 0$ V, indicating the existence of a fixed positive charge (Q_f) in the CeB_6/Al_2O_3 film.[21] In addition, it is calculated to be 4.0×10^{11} cm^{-2} based on formula (1).[21] Here, ΔW means the work function difference between H-diamond (4.9 eV) and Al (4.28 eV), and q is the electronic charge of 1.6×10^{-19} C. Furthermore, the ρ is deduced to be 4.1×10^{12} cm^{-2} obtained at a V_{GS} of -10 V based on $\int C dV_{GS}$.[20] Moreover, μ_{sat} is also investigated to evaluate the channel transport characteristics based on expression (2).[3] The μ_{sat} of the CeB_6/Al_2O_3 H-diamond FET is 593.6 cm^2/V s at a V_{GS} of -3 V,

$$I_{DSmax} = \frac{W_G}{2L_G} C_{GS}\mu_{sat}(V_{GS} - V_{TH})^2, \tag{1}$$

$$Q_f = \frac{V_{FB} - \Delta W/q}{q} C_{GS}. \tag{2}$$

In addition, to evaluate the interface characteristics of the device, the interface state density (D_{it}) is calculated to be 5.9×10^{12} cm^{-2} eV^{-1} based on the following expression:[22]

$$SS = (\ln 10)\frac{kT}{q}\frac{C_{GS} + C_D + qD_{it}}{C_{GS}}, \tag{3}$$

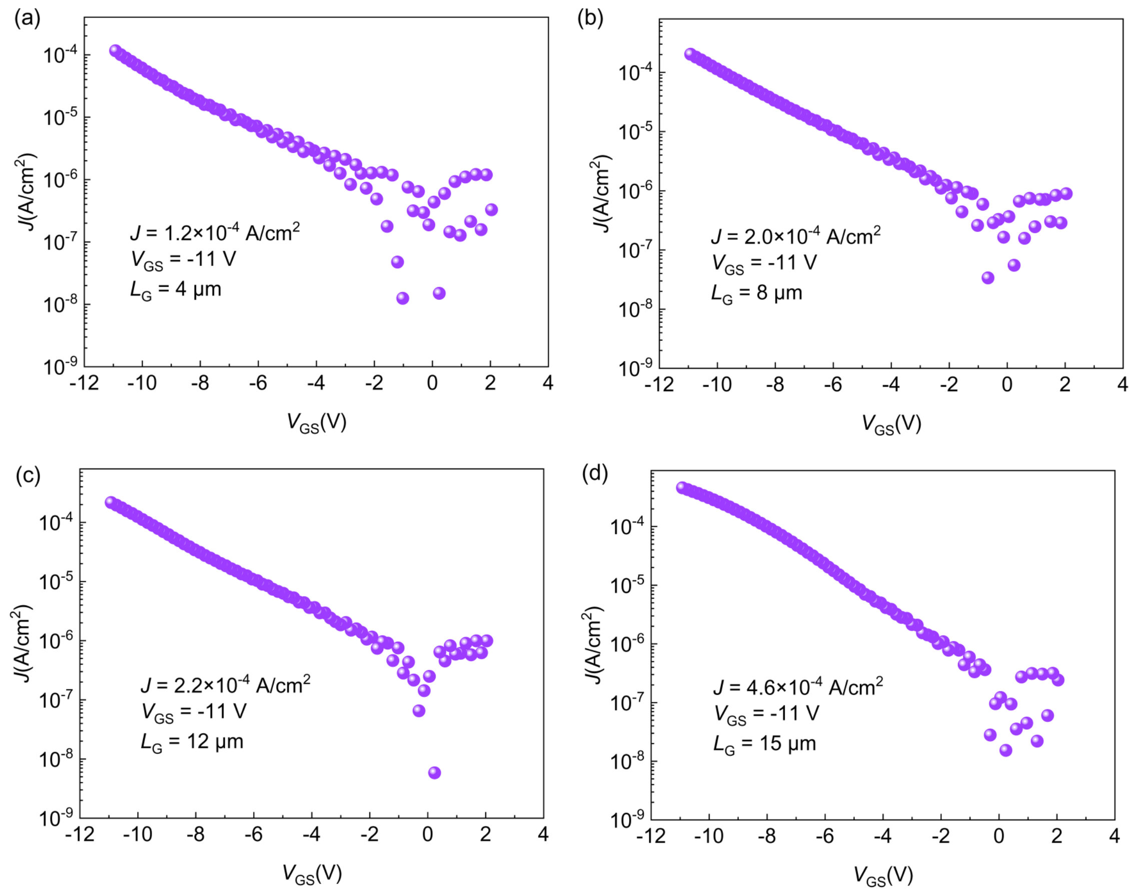

FIG. 8. J characteristics (J–V_{GS}) of the $Al/Al_2O_3/CeB_6$ H-diamond FET (a)–(d) with L_G of 4, 8, 12, and 15 μm, respectively.

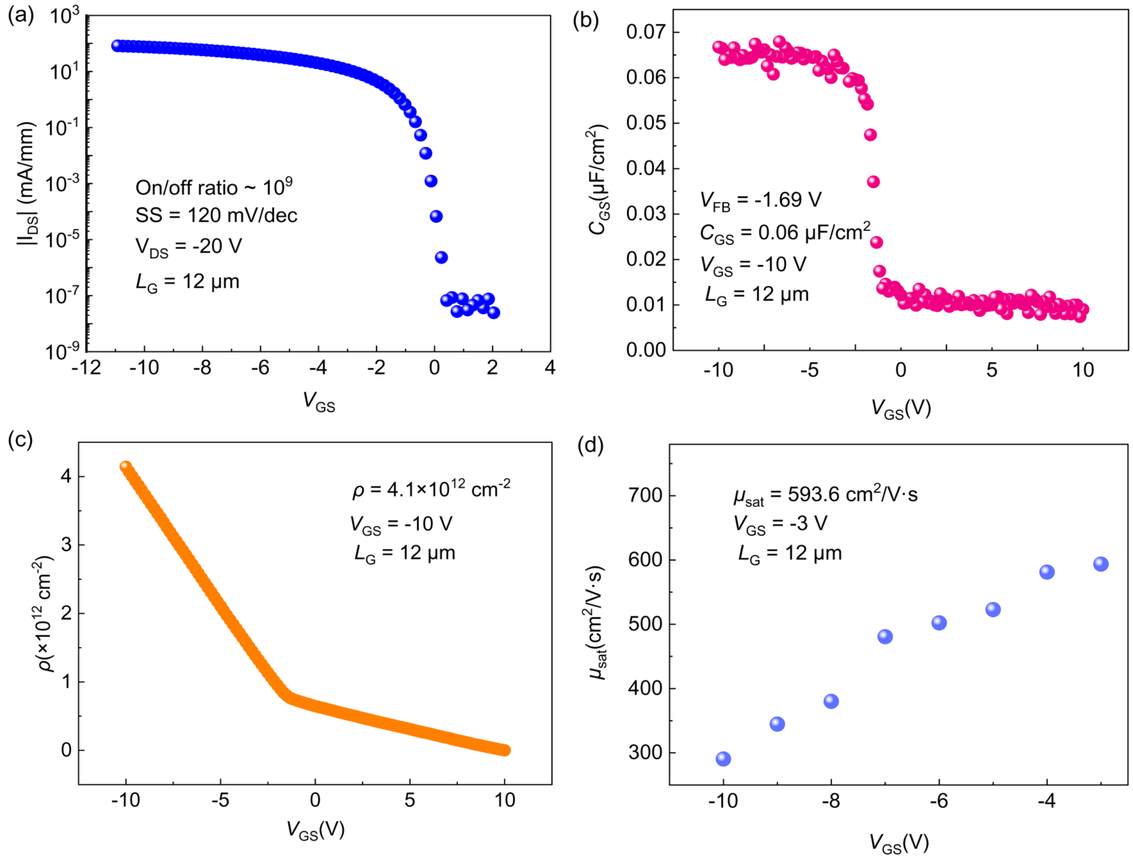

FIG. 9. Electrical properties of the $Al/Al_2O_3/CeB_6$ H-diamond FET with a L_G of 12 μm (a) $|I_{DS}| - V_{GS}$, (b) $C_{GS} - V_{GS}$, (c) $\rho - V_{GS}$, (d) $\mu_{sat} - V_{GS}$.

where k is the Boltzmann constant and C_D is the depletion capacitance that may be negligible since its value is much smaller than C_{GS}.[22]

Table I demonstrates the electrical properties' comparison with the reported H-diamond FETs. The hBN FET demonstrates excellent performances with a μ_{sat} of 680 cm^2/V s, yet the fabrication process is complicated.[1] The J of the Al_2O_3 FET is 4.46×10^{-6} A/cm^2 @$V_{GS} = -4$ V,[23] and for the Al_2O_3/CeB_6 FET in this work, J is 3.6×10^{-6} A/cm^2 @$V_{GS} = -4$ V. So, the two devices demonstrate similar J at the same V_{GS}. Compared with the CeB_6 FET, the J of the Al_2O_3/CeB_6 FET demonstrates competitive J. D_{it} for the hBN, CeB_6, and CeB_6/Al_2O_3 gate H-diamond FET are 6.8×10^{11}, 1.93×10^{12}, and 5.9×10^{12} cm^{-2} eV^{-1}, respectively. The D_{it} of hBN is low compared

TABLE I Electrical properties' comparison with the reported H-diamond FETs.

Gate materials	hBN	Al_2O_3	CeB_6	Al_2O_3/CeB_6
L_G (μm)	8.09	40	8	12
V_{TH} (V)	−0.99	…	−0.46	−0.4
I_{DSmax} (mA/mm)	−200	…	−83.8	−80.9
J (A/cm^2)	3×10^{-7}	4.46×10^{-6} @$V_{GS} = -4$ V	2.4×10^{-3} @$V_{GS} = -8$ V	2.2×10^{-4} @$V_{GS} = -11$ V
ρ (cm^{-2})	6.6×10^{12}	9.4×10^{12}	1.19×10^{13}	4.1×10^{12}
μ_{sat} (cm^2/V s)	680	94.2	260.5	593.6
D_{it} (cm^{-2} eV^{-1})	6.8×10^{11}	…	1.93×10^{12}	5.9×10^{12}
Ref.	1	23	15	This work

with other FETs, and this is a key factor for the high performance with a μ_{sat} of 680 cm^2/V s. D_{it} for the CeB_6 and Al_2O_3/CeB_6 FETs are all orders of magnitude 10^{12}.

IV. CONCLUSION

In conclusion, the H-diamond FET with Al_2O_3/CeB_6 gate materials has been fabricated and characterized. For the 4/8/12/15 μm L_G devices, all the devices demonstrate good electrical characteristics with I_{DSmax} of −114.6, −96.0, −80.9, and −73.7 mA/mm at a V_{DS} of −20 V and a V_{GS} of −11 V. V_{TH} are extracted to be −0.4, −0.5, −0.4, and −0.5 V, and this further verifies the effectiveness of the low work function material to realize normally off H-diamond FETs. All the J values are as low as 10^{-7} A/cm^2 at a V_{GS} of 0 V and 10^{-4} A/cm^2 at a V_{GS} of −11 V. For the 12 μm L_G devices, it exhibits a high on/off ratio of 10^9 and a large μ_{sat} of 593.6 cm^2/V s. In future work, the electrical properties will be further enhanced by optimizing the fabrication process, and this may significantly promote the application of normally off H-diamond FETs.

ACKNOWLEDGMENTS

This work was supported by the National Key Research and Development Program of China (No. 2022YFB3608603), the China Postdoctoral Science Foundation (No. 2022M712516), the Natural Science Basic Research Program of Shaanxi Province (No. 2023-JC-QN-0718), and the National Natural Science Foundation of China (NNSFC) (Nos. U21A2073, 62074127, 62304173, and 62304175).

AUTHOR DECLARATIONS

Conflict of Interest

The authors have no conflicts to disclose.

Author Contributions

Zhang Minghui: Conceptualization (lead); Data curation (lead); Methodology (lead); Software (lead); Validation (lead); Writing – original draft (lead). **Wang Wei:** Supervision (equal); Writing – review & editing (equal). **Chen Genqiang:** Formal analysis (lead); Methodology (supporting). **Wen Feng:** Resources (lead). **Lin Fang:** Investigation (lead). **Wang Yanfeng:** Software (supporting). **Zhang Pengfei:** Data curation (supporting). **Wang Fei:** Validation (supporting). **He Shi:** Formal analysis (supporting). **Liang Yuesong:** Formal analysis (equal). **Fan Shuwei:** Supervision (supporting). **Wang Kaiyue:** Investigation (supporting). **Yu Cui:** Project administration (equal). **Min Tai:** Project administration (equal). **Wang Hongxing:** Funding acquisition (lead); Supervision (supporting); Writing – review & editing (supporting).

DATA AVAILABILITY

The data that support the findings of this study are available from the corresponding author upon reasonable request.

REFERENCES

[1] Y. Sasama, T. Kageura, M. Imura, K. Watanabe, T. Taniguchi, T. Uchihashi, and Y. Takahide, Nat. Electron. **5**, 37 (2022).
[2] J. Isberg, J. Hammersberg, E. Johansson, T. Wikström, D. J. Twitchen, A. J. Whitehead, S. E. Coe, and G. A. Scarsbrook, Science **297**, 1670 (2002).
[3] M. Liao, L. Sang, T. Shimaoka, M. Imura, S. Koizumi, and Y. Koide, Adv. Electron. Mater. **5**, 1800832 (2019).
[4] Z. Minghui, W. Wei, W. Feng, L. Fang, C. Genqiang, W. Fei, H. Shi, W. Yanfeng, F. Shuwei, B. Renan, M. Tai, Y. Cui, and W. Hongxing, Funct. Diamond **2**, 258 (2022).
[5] H. Kawarada, Surf. Sci. Rep. **26**, 205 (1996).
[6] K. Hirama, H. Takayanagi, S. Yamauchi, Y. Jingu, H. Umezawa, and H. Kawarada, in *2007 IEEE International Electron Devices Meeting* (IEEE, New York, 2007), Vols. 1, 2, p. 873+.
[7] K. G. Crawford, I. Maini, D. A. Macdonald, and D. A. J. Moran, Prog. Surf. Sci. **96**, 100613 (2021).
[8] Z. Ren, S. Ding, Z. Liang, Q. He, K. Su, J. Zhang, J. Zhang, C. Zhang, and Y. Hao, Appl. Phys. Lett. **120**, 042104 (2022).
[9] K. Hirama, H. Sato, Y. Harada, H. Yamamoto, and M. Kasu, Jpn. J. Appl. Phys. **51**, 090114 (2012).
[10] C. Yu, C. Zhou, J. Guo, Z. He, M. Ma, H. Yu, X. Song, A. Bu, and Z. Feng, Funct. Diamond **2**, 64 (2022).
[11] M. Kasu, K. Ueda, H. Kageshima, and Y. Taniyasu, in *Physics Status Solidi C—Currents Top Solid State Physics*, edited by Y. Hirayama and T. Sogawa (Wiley-V C H Verlag Gmbh, Weinheim, 2008), Vol. 5, No. 9, pp. 3165–3168.
[12] X. Yu, J. Zhou, C. Qi, Z. Cao, Y. Kong, and T. Chen, IEEE Electron Device Lett. **39**, 1373 (2018).
[13] N. C. Saha, S. W. Kim, K. Koyama, T. Oishi, and M. Kasu, IEEE Electron Device Lett. **44** 10 (2022).
[14] M. Zhang, W. Wang, G. Chen, H. N. Abbasi, F. Lin, F. Wen, K. Wang, J. Zhang, R. Bu, and H. Wang, Appl. Phys. Lett. **118**, 5 (2021).
[15] M. Zhang, W. Wang, G. Chen, F. Wen, F. Lin, S. He, Y. Wang, L. Zhang, S. Fan, R. Bu, T. Min, C. Yu, and H. Wang, Carbon N. Y. **201**, 71 (2023).
[16] S. He, Y. F. Wang, G. Chen, M. Zhang, W. Wang, X. Chang, Q. Li, Q. Zhang, T. Zhu, and H. X. Wang, Diamond Relat. Mater. **120**, 6 (2021).
[17] R. G. Banal, M. Imura, J. Liu, and Y. Koide, J. Appl. Phys. **120**, 115307 (2016).
[18] J. W. Liu, M. Y. Liao, M. Imura, and Y. Koide, Appl. Phys. Lett. **103**, 092905 (2013).
[19] J. Liu, M. Liao, M. Imura, A. Tanaka, H. Iwai, and Y. Koide, Sci. Rep. **4**, 2 (2014).
[20] J. F. Zhang, W. J. Chen, Z. Y. Ren, K. Su, P. Z. Yang, Z. Z. Hu, J. C. Zhang, and Y. Hao, Phys. Status Solidi **217**, 1 (2020).
[21] J. W. Liu, H. Oosato, M. Y. Liao, and Y. Koide, Appl. Phys. Lett. **110**, 203502 (2017).
[22] T. Matsumoto, H. Kato, K. Oyama, T. Makino, M. Ogura, D. Takeuchi, T. Inokuma, N. Tokuda, and S. Yamasaki, Sci. Rep. **6**, 31585 (2016).
[23] Z. Ren, W. Chen, J. Zhang, J. Zhang, C. Zhang, G. Yuan, K. Su, Z. Lin, and Y. Hao, IEEE J. Electron Devices Soc. **7**, 88 (2019).